

## Early-phase $^{18}\text{F}$ -Florbetapir and $^{18}\text{F}$ -Flutemetamol images as proxies of brain metabolism in a memory clinic setting

Cecilia Boccalini <sup>1,2,3,\*</sup>, Débora Elisa Peretti <sup>1</sup>, Federica Ribaldi <sup>4,5</sup>, Max Scheffler <sup>6</sup>, Sara Stampacchia <sup>1</sup>, Szymon Tomczyk <sup>4</sup>, Cristelle Rodriguez <sup>7,8</sup>, Marie-Louise Montandon <sup>8,9</sup>, Sven Haller <sup>10,11,12,13</sup>, Panteleimon Giannakopoulos <sup>7,8</sup>, Giovanni B Frisoni <sup>4,5</sup>, Daniela Perani <sup>2,3,14</sup>, and Valentina Garibotto <sup>1,15,16</sup>

- (1) Laboratory of Neuroimaging and Innovative Molecular Tracers (NIMTlab), Geneva University Neurocenter and Faculty of Medicine, University of Geneva, Geneva, Switzerland
- (2) Vita-Salute San Raffaele University, Milan, Italy
- (3) In Vivo Human Molecular and Structural Neuroimaging Unit, Division of Neuroscience, IRCCS San Raffaele Scientific Institute, Milan, Italy
- (4) Laboratory of Neuroimaging of Aging (LANVIE), University of Geneva, Geneva, Switzerland
- (5) Memory Clinic, Geneva University Hospitals, Geneva, Switzerland
- (6) Division of Radiology, Diagnostic Department, Geneva University Hospitals, Geneva, Switzerland
- (7) Division of Institutional Measures, Medical Direction, University Hospitals of Geneva, Switzerland
- (8) Department of Psychiatry, Faculty of Medicine, University of Geneva, Switzerland
- (9) Department of Rehabilitation and Geriatrics, Geneva University Hospitals and University of Geneva, Switzerland
- (10) CIMC - Centre d'Imagerie Médicale de Cornavin, Geneva, Switzerland
- (11) Faculty of Medicine of the University of Geneva, Switzerland
- (12) Department of Surgical Sciences, Radiology, Uppsala University, Uppsala, Sweden
- (13) Department of Radiology, Beijing Tiantan Hospital, Capital Medical University, Beijing, 100070, P. R. China
- (14) Nuclear Medicine Unit, San Raffaele Hospital, Milan, Italy
- (15) Division of Nuclear Medicine and Molecular Imaging, Geneva University Hospitals, Geneva, Switzerland
- (16) CIBM Center for Biomedical Imaging, Geneva, Switzerland

**\*Correspondence to:**

Cecilia Boccalini,

Neuroimaging and Innovative Molecular Traces Lab, Hôpitaux Universitaires de Genève (HUG) & University of Genève, Rue Gabrielle-Perret-Gentil 4, CH-1205 Genève 14

In-vivo Human Molecular and Structural Neuroimaging Unit, Division of Neuroscience, San Raffaele Scientific Institute & Vita-Salute San Raffaele University, Via Olgettina 58, 20132 Milan, Italy

Orcid: 0000-0002-3518-436X

Tel. +39 02 2643 2708

E-mail: cecilia.boccalini@unige.ch

**Running title:** Early-phase amyloid-PET and  $^{18}\text{F}$ -FDG-PET

## ABSTRACT

Background: Alzheimer's disease (AD) neuropathologic changes are  $\beta$ -amyloid ( $A\beta$ ) deposition, pathologic tau, and neurodegeneration. Dual-phase amyloid-PET might be able to evaluate  $A\beta$  deposition and neurodegeneration with a single tracer injection. Early-phase amyloid-PET scans provide a proxy for cerebral perfusion, which has shown good correlations with neural dysfunction measured through metabolic consumption, while the late frames depict amyloid distribution. Our study aims to assess the comparability between early-phase amyloid-PET scans and  $^{18}\text{F}$ -fluorodeoxyglucose ( $^{18}\text{F}$ -FDG)-PET brain topography at the individual level, and their ability to discriminate patients.

Methods: 166 subjects evaluated at the Geneva Memory Center, ranging from cognitively unimpaired to Mild Cognitive Impairment (MCI) and dementia, underwent early-phase amyloid-PET – using either  $^{18}\text{F}$ -florbetapir (eFBP) (n=94) or  $^{18}\text{F}$ -flutemetamol (eFMM) (n=72) – and  $^{18}\text{F}$ -FDG-PET.  $A\beta$  status was assessed. Standardized uptake value ratios (SUVR) were extracted to evaluate the correlation of eFBP/eFMM and their respective  $^{18}\text{F}$ -FDG-PET scans. The single-subject procedure was applied to investigate hypometabolism and hypoperfusion maps and their spatial overlap by Dice coefficient. Receiver operating characteristic analyses were performed to compare the discriminative power of eFBP/eFMM, and  $^{18}\text{F}$ -FDG-PET SUVR in AD-related metaROI between  $A\beta$ -negative healthy controls and cases in the AD continuum.

Results: Positive correlations were found between eFBP/eFMM and  $^{18}\text{F}$ -FDG-PET SUVR independently of  $A\beta$  status and  $A\beta$  radiotracer ( $R > 0.72$ ,  $p < 0.001$ ). eFBP/eFMM single-subject analysis revealed clusters of significant hypoperfusion with good correspondence to hypometabolism topographies, independently of the underlying neurodegenerative patterns. Both eFBP/eFMM and  $^{18}\text{F}$ -FDG-PET SUVR significantly discriminated AD patients from controls in the AD-related metaROIs ( $AUC_{\text{FBP}} = 0.888$ ;  $AUC_{\text{FMM}} = 0.801$ ), with  $^{18}\text{F}$ -FDG-PET performing slightly better, however not significantly (all p-value higher than 0.05), than others ( $AUC_{\text{FDG}} = 0.915$  and  $0.832$  for subjects evaluated with  $^{18}\text{F}$ -FBP and  $^{18}\text{F}$ -FMM, respectively).

Conclusions: The distribution of perfusion was comparable to that of metabolism at the single-subject level by parametric analysis, particularly in the presence of a high neurodegeneration burden. Our findings indicate that eFBP/eFMM imaging can replace  $^{18}\text{F}$ -FDG-PET imaging, as they reveal typical neurodegenerative patterns, or allow to exclude the presence of neurodegeneration. The finding shows cost-saving capacities of amyloid-PET and supports the routine use of the modality for individual classification in clinical practice.

**Keywords:** neurodegeneration; early-phase amyloid-PET;  $^{18}\text{F}$ -fluorodeoxyglucose-PET; individual maps

## INTRODUCTION

Positron emission tomography (PET) can provide *in vivo* evaluation of protein deposition and neuronal injury (1), playing a leading role in the diagnosis of Alzheimer's disease (AD) and other dementia conditions. Brain  $^{18}\text{F}$ -fluorodeoxyglucose (FDG) PET scan is a well-established tool for investigating neurodegeneration, through the detection of changes in cerebral glucose metabolism. Regional analysis of  $^{18}\text{F}$ -FDG-PET signal can reveal specific brain hypometabolism patterns highly indicative of neurodegeneration along the AD, frontotemporal dementia (FTD), and Lewy-bodies spectrum, including subjects from the preclinical phases to clinically overt dementia (2). In longitudinal studies, the absence of disease-specific hypometabolism patterns was a strong predictor of preserved cognition (3–5).

Amyloid-PET imaging, initially with  $^{11}\text{C}$ -labeled Pittsburgh Compound B ( $^{11}\text{C}$ -PiB) and now also with three  $^{18}\text{F}$ -labelled compounds, namely  $^{18}\text{F}$ -florbetapir (FBP),  $^{18}\text{F}$ -florbetaben, and  $^{18}\text{F}$ -flutemetamol (FMM), allows the assessment of A $\beta$  plaque burden *in vivo* (1). A dual-phase amyloid-PET protocol of acquisition has been proposed, adding to the reference “late” acquisition, the acquisition of the tracer distribution immediately after injection (6). These early-phase images can provide a proxy for cerebral perfusion because of the high lipophilicity of the tracers (6,7). In turn, cerebral perfusion is strongly related to neural dysfunction as measured through metabolic consumption (8,9). In AD, the early-phase acquisition of amyloid-PET has shown a good correlation to  $^{18}\text{F}$ -FDG-PET uptake at group level, suggesting its potential use as a biomarker of neuronal dysfunction (10–21).

Despite multiple descriptions in the literature of dual-phase amyloid-PET, the use of early-phase images in clinical and research settings is not yet widely implemented. Our study explores the utility of early-phase images of amyloid-PET scans, using either  $^{18}\text{F}$ -FBP or  $^{18}\text{F}$ -FMM, for individual classification, and their comparability with the respective  $^{18}\text{F}$ -FDG-PET brain hypometabolic voxel-wise maps, in a memory clinic cohort.

## **MATERIALS AND METHODS**

### **Participants**

The study included subjects assessed at the Geneva University Hospitals, ranging from cognitively unimpaired (CU) to Mild Cognitive Impairment (MCI) and dementia, in two ongoing studies as described previously (22–26). The local ethics committee approved the different imaging studies, which have been conducted under the principles of the Declaration of Helsinki and the International Conference on Harmonization Good Clinical Practice. Thus, the institutional review board (IRB or equivalent) approved this study and the requirement to obtain informed consent was waived.

We included a total of 166 subjects classified as amyloid-negative CU (N=42), amyloid-positive CU (N=30), MCI (N=73) (27), and dementia (28) (N=21) subjects, following standardized criteria for clinical staging. Specifically, the amyloid-negative CU group, including healthy volunteers and individuals with subjective cognitive decline (29), all with  $^{18}\text{F}$ -FDG-PET negative scans, was used as healthy control (HC) reference for comparisons. Amyloid-positive CU, instead, were considered a group of interest, given the higher risk of progression in this population (30). Inclusion criteria were: (i) at least one 3D T1 MRI scan, (ii) dual-phase amyloid-PET using either  $^{18}\text{F}$ -FBP or  $^{18}\text{F}$ -FMM, (iii) an  $^{18}\text{F}$ -FDG-PET scan, and (iv) a time interval between imaging measures shorter than one year.

### **MRI acquisition**

Magnetic resonance imaging (MRI) was performed at Geneva University Hospitals' Division of Radiology using a 3 Tesla scanner (Magnetom Skyra, Siemens Healthineers, Erlangen, Germany), equipped with a 20- or 64-channel head coil. See Supplemental Materials (1) for acquisition parameters details. Lesion Prediction Algorithm (31), implemented in Lesion Segmentation Toolbox, was used to segment FLAIR images, allowing us to extract the total lesion volume (TLV). White matter lesions were quantified also visually according to the age-related white matter changes scale (ARWMC) (32).

## **PET acquisition**

$^{18}\text{F}$ -FDG-PET and amyloid-PET scans were performed at the nuclear medicine and molecular imaging division at Geneva University Hospitals with Biograph128 mCT, Biograph128 Vision 600 Edge, Biograph40 mCT, or Biograph64 TruePoint PET scanners (Siemens Medical Solutions, USA). All scanners were comparable.

$^{18}\text{F}$ -FDG-PET was performed according to the European Association of Nuclear Medicine (EANM) guidelines (33,34).

Amyloid-PET images were acquired using  $^{18}\text{F}$ -FBP (n = 94) or  $^{18}\text{F}$ -FMM (n = 72) tracers. Amyloid status (A $\beta$ + / A $\beta$ -) was determined for each late image by an expert in nuclear medicine (VG) applying the standard operating procedures approved by the European Medicines Agency.

Regarding the early-phase of amyloid-PET (eFBP and eFMM), the image acquisition was started immediately after tracer injection and a static image was acquired for 5 minutes (eFBP) or 10 minutes (eFMM) (20,35).

See Supplemental Materials (2) for full details on PET acquisition.

## **MRI and PET normalization processing**

Processing was performed according to (25) using Statistical Parametric Mapping (SPM 12, Wellcome Trust Centre for Neuroimaging, London, UK), running in MATLAB R2018b Version 9.5 (MathWorks Inc., Sherborn, MA, USA). All details are reported in Supplemental Materials (3).

## **SUVr extraction in AAL ROIs and AD metaROIs**

Uptake values were extracted within regions from the automated anatomical labelling (AAL) atlas 3 (36) and key regions sensitive to AD according to a predefined metaROI approach (37). Standardized uptake value ratios (SUVr) were calculated by normalizing the uptake to the mean value of the pons and cerebellar

vermis together as the reference region. Intensity normalized PET images were saved for further voxel-wise analyses.

### **Single-subject voxel-wise analyses**

According to a validated SPM single-subject procedure (38), each PET image was tested for relative hypometabolism/hypoperfusion by means of a two-sample t-test in comparison with PET images of controls. HC groups included 28 and 14 subjects with A $\beta$ - and <sup>18</sup>F-FDG-PET negative scans, for FBP and FMM samples, respectively. We used the same HC subjects also for the <sup>18</sup>F-FDG-PET analyses. The statistical threshold for the resulting hypometabolic and hypoperfusion SPM maps was set at  $p = 0.05$  uncorrected for multiple comparisons, considering significant clusters containing more than 100 voxels. SPM maps were then binarized for further Dice analyses. The resulting single-subject SPM hypometabolic maps were visually inspected by nuclear medicine experts (DP and VG) blinded to clinical diagnoses, and classified into hypometabolism patterns suggestive of neurodegenerative conditions (3,39–41) or excluding the presence of neurodegeneration. Hypometabolic and hypoperfusion maps were all visually inspected at the single-subject level to define the visual match between maps. The same assessment has been applied also to <sup>18</sup>F-FDG-PET and eFBP/eFMM uptake distribution images.

### **Statistical analyses**

Dice coefficient was calculated, using FSL software (42), to quantify the whole-brain spatial overlap between hypometabolic and hypoperfusion binary maps at the single-subject level (43) (Supplemental Materials 4). Moreover, we calculated delta scores between the hypometabolic and hypoperfusion maps' extents (number of voxels) to quantify discrepancies between the two patterns.

General linear models were performed to assess the correlation between eFBP/eFMM SUVR in the AAL ROIs and their respective <sup>18</sup>F-FDG SUVR in the whole sample. We assessed the correlations also in A $\beta$ + and A $\beta$ - subjects separately. We tested the correlation of eFBP, eFMM, and <sup>18</sup>F-FDG SUVR in the AD composite metaROI with MMSE scores.

Finally, we identified patients in the AD continuum including specifically MCI and AD dementia (ADD) cases according to the A $\beta$ + status and AD-like hypometabolism patterns. We performed receiver operating characteristic (ROC) analyses to compare the discriminative power of eFBP, eFMM, and <sup>18</sup>F-FDG MetaROIs SUVR between HC and AD patients. The resulting areas under the curve (AUC) from different tracers were compared using a De Long test (44) for 2 correlated ROC curves, setting the threshold for significance at a *p*-value of 0.05. All statistical analyses were performed with R, version 4.0.2 (R Foundation for statistical computing, <https://www.r-project.org/>).

## RESULTS

Demographic and clinical data for our cohort are displayed in Table 1.

The average time intervals between amyloid-PET and <sup>18</sup>F-FDG-PET, between MRI and <sup>18</sup>F-FDG-PET, and between MRI and amyloid-PET were 2.15 months (SD=3.06), 1.89 months (SD=4.15), and 2.76 months (SD=3.40), respectively.

### Correlations between early FBP/FMM and <sup>18</sup>F-FDG SUVR

Both eFBP and eFMM SUVR in the AAL ROIs presented a strong correlation with <sup>18</sup>F-FDG SUVR in the whole group ( $R_{\text{FBP}}=0.786$ ,  $p<0.001$ ;  $R_{\text{FMM}}=0.806$ ,  $p<0.001$ ). Good correlations between eFBP/eFMM and <sup>18</sup>F-FDG SUVR were also found separately in A $\beta$ + ( $R_{\text{FBP}}=0.843$ ,  $p<0.001$ ;  $R_{\text{FMM}}=0.827$ ,  $p<0.001$ ) and A $\beta$ - ( $R_{\text{FBP}}=0.72$ ,  $p<0.001$ ;  $R_{\text{FMM}}=0.791$ ,  $p<0.001$ ) subjects. Figure 1 shows scatter plots for the whole sample and subgroups according to A $\beta$  status.

The composite metaROI SUVRs for eFBP/eFMM uptake and those for <sup>18</sup>F-FDG uptake were significantly correlated with MMSE scores ( $R_{\text{FDG}}=0.536$ ,  $p<0.001$ ;  $R_{\text{FBP}}=0.413$ ,  $p<0.001$ ;  $R_{\text{FMM}}=0.482$ ,  $p<0.001$ ).

### Single-subject early FBP/FMM and <sup>18</sup>F-FDG patterns

The SPM single-subject analysis revealed disease-specific hypometabolism and hypoperfusion maps (Figure 2, Tables 2 and 3). See Supplemental Materials (5) and Supplemental Tables 1, 2, 3 for the results



of visual analyses for the uptake distribution images. The visual rating of SPM maps allowed to identify four neurodegenerative patterns: a) temporoparietal hypometabolism (AD-like pattern, N=39); b) temporoparietal and occipital hypometabolism (Lewy-bodies (DLB)-like pattern, N=3); c) frontotemporal hypometabolism (FTD-like pattern, N=10); and d) limbic-like or medial-temporal pattern (N=14). 32 out of 124 subjects showed negative  $^{18}\text{F}$ -FDG scans for neurodegenerative patterns. Some subjects revealed severe atrophy at T1 MRI and not classifiable SPM patterns for neurodegenerative disease (N=26). Despite this heterogeneity, for 86% of subjects, the patterns identified by  $^{18}\text{F}$ -FDG-PET were consistently found in early-phase maps at visual assessment. The frequency of the different hypometabolism and hypoperfusion patterns classified on the basis of the interpretation of the SPM maps is reported in Table 2. Table 3 shows the frequency of hypometabolism patterns and their spatial overlaps with hypoperfusion maps as measured by Dice and visual assessment, in the whole sample and separately in the three clinical subgroups (CU, MCI, Dementia). The hypometabolic/hypoperfusion maps resulting in the three clinical subgroups are fully detailed in Supplemental Materials (6).

Only 16 out of 124 subjects (13%) showed a mismatch between  $^{18}\text{F}$ -FDG and eFBP/eFMM scans. When we compared MRI TLV and ARWMC scores between the matched and mismatched subgroups, we found a more severe cerebrovascular pathology in cases with mismatch compared to matched cases (Mann-Whitney  $U = 384$ ,  $p=0.021$ ;  $U = 431$ ,  $p=0.041$ ; for TLV and ARWMC, respectively).

When we calculated delta scores to explore discrepancies between the eFBP/eFMM and  $^{18}\text{F}$ -FDG-PET maps, the main difference was found in the extent of the abnormalities. 65 out of 92 subjects showed positive delta scores indicating the hypometabolism patterns more extended than the hypoperfusion ones (delta scores= $13012 \pm 12996$  voxels), regardless of the clinical category. Only 27 out of 92 subjects presented negative delta scores indicating hypoperfusion patterns slightly more extended than the hypometabolic ones (delta scores =  $-6606 \pm 6943$  voxels).

## **Discriminative performance of AD metaROI approach**

When testing the performance of the eFBP/eFMM SUVR in AD composite metaROI in distinguishing AD patients from HC, we found good AUC discriminative values ( $AUC_{FBP}=0.888$ ,  $AUC_{FMM}=0.801$ ), like that of the  $^{18}\text{F}$ -FDG SUVR ( $AUC_{FDG}=0.915$  and  $0.832$ , respectively). DeLong test confirmed no significant differences in the discriminatory performance of different tracers ( $p_{FDG \text{ vs FBP}}=0.396$  and  $p_{FDG \text{ vs FMM}}=0.665$ ). Figure 3 compares the diagnostic performance of  $^{18}\text{F}$ -FDG-PET SUVR and eFBP/eFMM SUVR in composite AD metaROI in terms of ROC curves for the whole AD continuum group.

As for the other AD-related metaROIs (37), none of them presented significant differences in the discriminatory power of  $^{18}\text{F}$ -FDG-PET and eFBP/eFMM SUVR between AD patients versus HC (Supplemental Table 4).

## **DISCUSSION**

This study compared early-phase amyloid-PET with  $^{18}\text{F}$ -FDG-PET patterns and the power to discriminate subjects in the AD continuum and with other neurodegenerative conditions from HC. The correlation between cerebral perfusion and metabolism has been long-established in aging and dementia conditions based on neurovascular coupling (8). At the same time, early acquisition images of amyloid-PET have been proposed as a topographical/functional biomarker reflecting cerebral perfusion (6).

Dual-phase amyloid-PET may thus offer the advantage of acquiring information about amyloidosis and brain perfusion deficits reflecting neurodegeneration with a single procedure (6). Published work has focused on the relationship between brain perfusion and metabolism at group level, but no studies have so far evaluated whether early-phase images could replace  $^{18}\text{F}$ -FDG-PET images in single individuals. This study evaluated the brain hypoperfusion at the single-subject level and its comparability to respective brain hypometabolism, demonstrating good correlation and similar capacity in distinguishing patients from controls. In the presence of neurodegeneration assessed by  $^{18}\text{F}$ -FDG-PET, eFBP/eFMM single-subject analysis showed clusters of significant hypoperfusion, compared to controls, with good correspondence to

the brain hypometabolism topography. The spatial overlap showed to be independent of underlying neurodegeneration topography, however, with a more clear-cut correspondence in the dementia stages (Figure 2).

In line with previous studies (10–18), our study confirms strong positive correlations between eFBP/eFMM and  $^{18}\text{F}$ -FDG SUVR ( $R>0.72$ ,  $p<0.001$ ) in a memory clinic cohort (Figure 1). The correlation was independent of the used  $\text{A}\beta$  radiotracers and amyloid status, in agreement with other studies (10,11,13,15). Further supporting the comparability between the eFBP/eFMM and  $^{18}\text{F}$ -FDG-PET images, we found that lower MMSE scores were significantly correlated with decreases in both perfusion and metabolism measures (10,12,13,16).

When we applied the SPM single-subject analysis on eFBP/eFMM images, clusters of significant hypoperfusion were present in patients compared to controls, with good correspondence to the hypometabolism maps (Figure 2 and Table 2). As for negative scans, characterizing mostly the CU and MCI subgroups, the perfusion maps' ability was comparable to that of metabolism maps in excluding the presence of neurodegeneration for the 90% of negative scans. In the sample of CU, we found 60%  $^{18}\text{F}$ -FDG-PET negative scans and, for 94% of these, eFBP/eFMM images agreed on ruling out neurodegenerative patterns.

In MCI, eFBP/eFMM maps were able to identify patterns specific to neurodegenerative conditions for most cases, showing a moderate-to-good degree of overlap with hypometabolism patterns (Table 3). In most cases, hypometabolism SPM maps showed a greater extent than the hypoperfusion ones, although the disease-specific hallmark was detectable in both (Figure 2). The lack of a full overlap here between perfusion and metabolism maps is likely due to their measures of the different brain biological processes (8,17). Other reasonable explanations are the noisy feature of the initial frames and the non-uniform delivery of the tracer (13). However, although the early-phase image may be noisier, the similarity between the patterns is striking also in MCI conditions supporting its utilization (Figure 2). A negative  $^{18}\text{F}$ -FDG-

PET scan in MCI was confirmed in 86% of eFBP/eFMM images. This is compatible with the absence of neurodegeneration in MCI, followed by a stable condition at follow-up (45,46).

In dementia conditions, the high comparability of hypoperfusion and hypometabolism maps suggests an increase in concordance with the advance of disease stages (Figure 2B). Since hypoperfusion usually showed less extension than hypometabolism maps, a more severe underlying neurodegeneration may be necessary to reveal specific patterns that are instead detectable with  $^{18}\text{F}$ -FDG-PET. This finding suggests that  $^{18}\text{F}$ -FDG-PET might be more suitable for preclinical and prodromal stages. Further studies are needed to specifically address preclinical phases, such as Subjective Cognitive Decline, based on larger samples and follow-up data.

We found only 13% of subjects with a mismatch between hypometabolism and hypoperfusion maps in the whole sample, mostly in the CU and MCI groups. In these cases, the eFBP/eFMM images were less sensitive to detect the underlying neurodegeneration than  $^{18}\text{F}$ -FDG-PET. The risk of finding false-negative scans with early-phase imaging warrants an additional  $^{18}\text{F}$ -FDG-PET exam when the clinical suspicion of neurodegenerative conditions is high. The group of mismatch cases showed greater cerebrovascular lesion volumes on MRI compared to the match group. This result is consistent with the fact that both  $^{18}\text{F}$ -FDG-PET and eFBP/eFMM images can suffer from biases in presence of severe atrophy and/or cerebral vascular disease (8). Thus, this limitation needs to be considered in the application and interpretation of SPM analysis both with  $^{18}\text{F}$ -FDG-PET and early-phase imaging.

Finally, we found a good diagnostic performance of the metaROI approach using perfusion measures (Figure 3). Both eFBP and eFMM SUVR in the composite metaROI significantly discriminated AD patients from HC. At ROC analyses,  $^{18}\text{F}$ -FDG SUVR was slightly superior in discriminating these subjects from controls than perfusion measures, however without reaching the significance threshold for differences ( $p>0.05$ ) (Figure 3).

As a limitation of our study, we acquired the early-phase images using published protocols (20), however, different timings have also been proposed in the literature as the optimal early time frames of eFBP to

achieve the best association with  $^{18}\text{F}$ -FDG-PET (16,18). We are aware of the relatively limited sample size of HC included for comparisons; further studies will help to confirm the findings. An appropriate normalization procedure and HC dataset are mandatory to achieve good performances in voxel-wise analyses and methods for early-phase images are in this respect less mature than for  $^{18}\text{F}$ -FDG-PET (47).

## **CONCLUSIONS**

This is the first study that evaluates, at the single-subject level by applying voxel-based analysis, the classification performance of early-phase amyloid-PET images. eFBP and eFMM imaging is able in identifying different and typical neurodegenerative patterns – or excluding the presence of neurodegeneration. Dual-phase amyloid PET permits assessing neurodegeneration and amyloid pathology with a single tracer injection and should be systematically implemented in routine clinical practice. In our opinion, in cases of discrepancy between clinical and imaging results, mainly in the early phase of the disease, an additional  $^{18}\text{F}$ -FDG-PET exam is recommended.

## **DISCLOSURE**

All authors disclose that they have no conflict of interest.

## **FUNDING INFORMATION**

PET scans were performed within research projects funded by the Swiss National Science Foundation (SNSF, project numbers: 320030\_169876 and 320030\_182772); Horizon 2020 (projects n. 667375); Human Brain Project; and the EU-EFPIA Innovative Medicines Initiatives 2 Joint Undertaking (IMI 2 JU; grant agreement number: 115952 and 115736). This project was funded in part by a grant of the Swiss National Science Foundation SNF 3200B0-1161193 and SPUM 33CM30- 124111 and an unrestricted grant from the Association pour la Recherche sur l'Alzheimer, Geneva, Switzerland. The Centre de la mémoire at Geneva University Hospital, collecting data with contributions of the Clinical Research Center (University Hospital and Faculty of Medicine, Geneva) is funded by private donors: Association Suisse pour la Recherche sur l'Alzheimer, Genève; Fondation Segré, Genève; Ivan Pictet, Genève; Fondazione Agusta, Lugano; Fondation Chmielewski, Genève; Velux Stiftung.

## **KEY POINTS**

Question: Can we use early-phase amyloid-PET scans instead of  $^{18}\text{F}$ -FDG-PET for individual classification?

Pertinent findings: i) the single-subject procedure applied to early-phase amyloid-PET provide typical neurodegenerative patterns in patients as compared to controls, especially in the advanced stage of the diseases; ii) the topographical similarity between the hypoperfusion and hypometabolic patterns is striking supporting their utilization for individual classification; iii) early-phase amyloid-PET imaging can exclude the presence of neurodegeneration.

Implication for patient care: Dual-phase amyloid-PET permits assessing neurodegeneration and amyloid pathology with a single tracer injection in one exam and its implementation will be optimal in terms of costs, patient comfort, and radiation exposure.

## REFERENCES

1. Villemagne VL, Barkhof F, Garibotto V, Landau SM, Nordberg A, van Berckel BNM. Molecular imaging approaches in dementia. *Radiology*. 2021;298:517-530.
2. Perani D, Caminiti SP, Carli G, Tondo G. PET Neuroimaging in Dementia Conditions. *PET SPECT Neurol*. 2020:211-282.
3. Cerami C, Della Rosa PA, Magnani G, et al. Brain metabolic maps in Mild Cognitive Impairment predict heterogeneity of progression to dementia. *NeuroImage Clin*. 2015;7:187-194.
4. Ossenkoppele R, Prins ND, Pijnenburg YAL, et al. Impact of molecular imaging on the diagnostic process in a memory clinic. *Alzheimer's Dement*. 2013;9:414-421.
5. Silverman DHS, Mosconi L, Ercoli L, Chen W, Small GW. Positron Emission Tomography scans obtained for the evaluation of cognitive dysfunction. *Semin Nucl Med*. 2008;38:251-261.
6. Garibotto V, Morbelli S, Pagani M. Dual-phase amyloid PET: hitting two birds with one stone. *Eur J Nucl Med Mol Imaging*. 2016;43:1300-1303.
7. Gjedde A, Aanerud J, Braendgaard H, Rodell AB. Blood-brain transfer of Pittsburgh compound B in humans. *Front Aging Neurosci*. 2013;5:1-9.
8. Silverman DHS. Brain 18F-FDG PET in the diagnosis of neurodegenerative dementias: Comparison with perfusion SPECT and with clinical evaluations lacking nuclear imaging. *J Nucl Med*. 2004;45:594-607.
9. Jueptner M, Weiller C. Does measurement of regional cerebral blood flow reflect synaptic activity?—Implications for PET and fMRI. *Neuroimage*. 1995;2:148-156.
10. Tiepolt S, Hesse S, Patt M, et al. Early [18F]florbetaben and [11C]PiB PET images are a surrogate biomarker of neuronal injury in Alzheimer's disease. *Eur J Nucl Med Mol Imaging*. 2016;43:1700-

1709.

11. Seiffert AP, Gómez-Grande A, Villarejo-Galende A, et al. High correlation of static first-minute-frame (Fmf) pet imaging after 18f-labeled amyloid tracer injection with [18f]fdg pet imaging. *Sensors*. 2021;21:1-14.
12. Meyer PT, Hellwig S, Amtage F, et al. Dual-biomarker imaging of regional cerebral amyloid load and neuronal activity in dementia with PET and 11C-Labeled Pittsburgh compound B. *J Nucl Med*. 2011;52:393-400.
13. Rostomian AH, Madison C, Rabinovici GD, Jagust WJ. Early 11C-PIB frames and 18F-FDG PET measures are comparable: A study validated in a cohort of AD and FTLD patients. *J Nucl Med*. 2011;52:173-179.
14. Rodriguez-Vieitez E, Leuzy A, Chiotis K, Saint-Aubert L, Wall A, Nordberg A. Comparability of [18F]THK5317 and [11C]PIB blood flow proxy images with [18F]FDG positron emission tomography in Alzheimer's disease. *J Cereb Blood Flow Metab*. 2017;37:740-749.
15. Daerr S, Brendel M, Zach C, et al. Evaluation of early-phase [18F]-florbetaben PET acquisition in clinical routine cases. *NeuroImage Clin*. 2017;14:77-86.
16. Ottoy J, Verhaeghe J, Niemantsverdriet E, et al. 18F-FDG PET, the early phases and the delivery rate of 18F-AV45 PET as proxies of cerebral blood flow in Alzheimer's disease: Validation against 15O-H2O PET. *Alzheimer's Dement*. 2019;15:1172-1182.
17. Peretti DE, García DV, Reesink FE, et al. Relative cerebral flow from dynamic PIB scans as an alternative for FDG scans in Alzheimer's disease PET studies. *PLoS One*. 2019;14:1-19.
18. Vanhoutte M, Landeau B, Sherif S, et al. Evaluation of the early-phase [18F]AV45 PET as an optimal surrogate of [18F]FDG PET in ageing and Alzheimer's clinical syndrome. *NeuroImage Clin*. 2021;31:1-15.



19. Forsberg A, Engler H, Blomquist G, Långström B, Nordberg A. The use of PIB-PET as a dual pathological and functional biomarker in AD. *Biochim Biophys Acta - Mol Basis Dis.* 2012;1822:380-385.
20. Hsiao IT, Huang CC, Hsieh CJ, et al. Correlation of early-phase 18F-florbetapir (AV-45/Amyvid) PET images to FDG images: Preliminary studies. *Eur J Nucl Med Mol Imaging.* 2012;39:613-620.
21. Rodriguez-Vieitez E, Carter SF, Chiotis K, et al. Comparison of early-phase 11C-Deuterium-L-Deprenyl and 11C-Pittsburgh Compound B PET for Assessing Brain Perfusion in Alzheimer Disease. *J Nucl Med.* 2016;57:1071-1077.
22. Montandon ML, Herrmann FR, Garibotto V, Rodriguez C, Haller S, Giannakopoulos P. Determinants of mesial temporal lobe volume loss in older individuals with preserved cognition: a longitudinal PET amyloid study. *Neurobiol Aging.* 2020;87:108-114.
23. Giannakopoulos P, Rodriguez C, Montandon ML, Garibotto V, Haller S, Herrmann FR. Less agreeable, better preserved? A PET amyloid and MRI study in a community-based cohort. *Neurobiol Aging.* 2020;89:24-31.
24. Zanchi D, Montandon ML, Sinanaj I, et al. Decreased fronto-parietal and increased default mode network activation is associated with subtle cognitive deficits in elderly controls. *NeuroSignals.* 2018;25:127-138.
25. Dodich A, Mendes A, Assal F, et al. The A/T/N model applied through imaging biomarkers in a memory clinic. *Eur J Nucl Med Mol Imaging.* 2020;47:247-255.
26. Frisoni GB, Barkhof F, Altomare D, et al. AMYPAD Diagnostic and Patient Management Study: Rationale and design. *Alzheimer's Dement.* 2019;15:388-399.
27. Albert MS, DeKosky ST, Dickson D, et al. The diagnosis of mild cognitive impairment due to Alzheimer's disease: recommendations from the National Institute on Aging-Alzheimer's

- Association workgroups on diagnostic guidelines for Alzheimer's disease. *Alzheimer's Dement.* 2011;7:270-279.
28. McKhann GM, Knopman DS, Chertkow H, et al. The diagnosis of dementia due to Alzheimer's disease: Recommendations from the National Institute on Aging-Alzheimer's Association workgroups on diagnostic guidelines for Alzheimer's disease. *Alzheimer's Dement.* 2011;7:263-269.
  29. Ribaldi F, Chicherio C, Altomare D, et al. Brain connectivity and metacognition in persons with subjective cognitive decline (COSCODE): rationale and study design. *Alzheimer's Res Ther.* 2021;13:1-8.
  30. Jessen F, Amariglio RE, Buckley RF, et al. The characterisation of subjective cognitive decline. *Lancet Neurol.* 2020;19:271-278.
  31. Schmidt P. Bayesian inference for structured additive regression models for large-scale problems with applications to medical imaging. Dissertation, LMU München: Faculty of Mathematics, Computer Science and Statistics. 2016:Chapter 6.1.
  32. Wahlund LO, Barkhof F, Fazekas F, et al. A new rating scale for age-related white matter changes applicable to MRI and CT. *Stroke.* 2001;32:1318-1322.
  33. Guedj E, Varrone A, Boellaard R, et al. EANM procedure guidelines for brain PET imaging using [18F]FDG, version 3. *Eur J Nucl Med Mol Imaging.* 2021.
  34. Boellaard R, Delgado-Bolton R, Oyen WJG, et al. FDG PET/CT: EANM procedure guidelines for tumour imaging: version 2.0. *Eur J Nucl Med Mol Imaging.* 2015;42:328-354.
  35. Schmitt J, Palleis C, Sauerbeck J, et al. Dual-Phase  $\beta$ -Amyloid PET Captures Neuronal Injury and Amyloidosis in Corticobasal Syndrome. *Front Aging Neurosci.* 2021;13.
  36. Rolls ET, Huang CC, Lin CP, Feng J, Joliot M. Automated anatomical labelling atlas 3.

- Neuroimage*. 2020;206:116189.
37. Landau SM, Harvey D, Madison CM, et al. Associations between cognitive, functional, and FDG-PET measures of decline in AD and MCI. *Neurobiol Aging*. 2011;32:1207-1218.
  38. Perani D, Anthony P, Rosa D, et al. Validation of an optimized SPM procedure for FDG-PET in dementia diagnosis in a clinical setting. *NeuroImage Clin*. 2014;6:445-454.
  39. Caminiti SP, Ballarini T, Sala A, et al. FDG-PET and CSF biomarker accuracy in prediction of conversion to different dementias in a large multicentre MCI cohort. *NeuroImage Clin*. 2018;18:167-177.
  40. Tondo G, Carli G, Santangelo R, et al. Biomarker-based stability in limbic-predominant amnesic mild cognitive impairment. *Eur J Neurol*. 2020:0-3.
  41. Teune LK, Bartels AL, De Jong BM, et al. Typical cerebral metabolic patterns in neurodegenerative brain diseases. *Mov Disord*. 2010;25:2395-2404.
  42. Jenkinson M, Beckmann CF, Behrens TEJ, Woolrich MW, Smith SM. Fsl. *Neuroimage*. 2012;62:782-790.
  43. Savio A, Fänger S, Tahmasian M, et al. Resting-state networks as simultaneously measured with functional MRI and PET. *J Nucl Med*. 2017;58:1314-1317.
  44. DeLong ER, DeLong DM, Clarke-Pearson DL. Comparing the areas under two or more correlated receiver operating characteristic curves: a nonparametric approach. *Biometrics*. 1988:837-845.
  45. Pandya SY, Clem MA, Silva LM, Woon FL. Does mild cognitive impairment always lead to dementia? A review. *J Neurol Sci*. 2016;369:57-62.
  46. Petersen RC, Lopez O, Armstrong MJ, et al. Practice guideline update summary: Mild cognitive impairment report of the guideline development, dissemination, and implementation. *Neurology*.

2018;90:126-135.

47. Della Rosa PA, Cerami C, Gallivanone F, et al. A standardized [18 F]-FDG-PET template for spatial normalization in statistical parametric mapping of dementia. *Neuroinformatics*. 2014;12:575-593.

## Figures

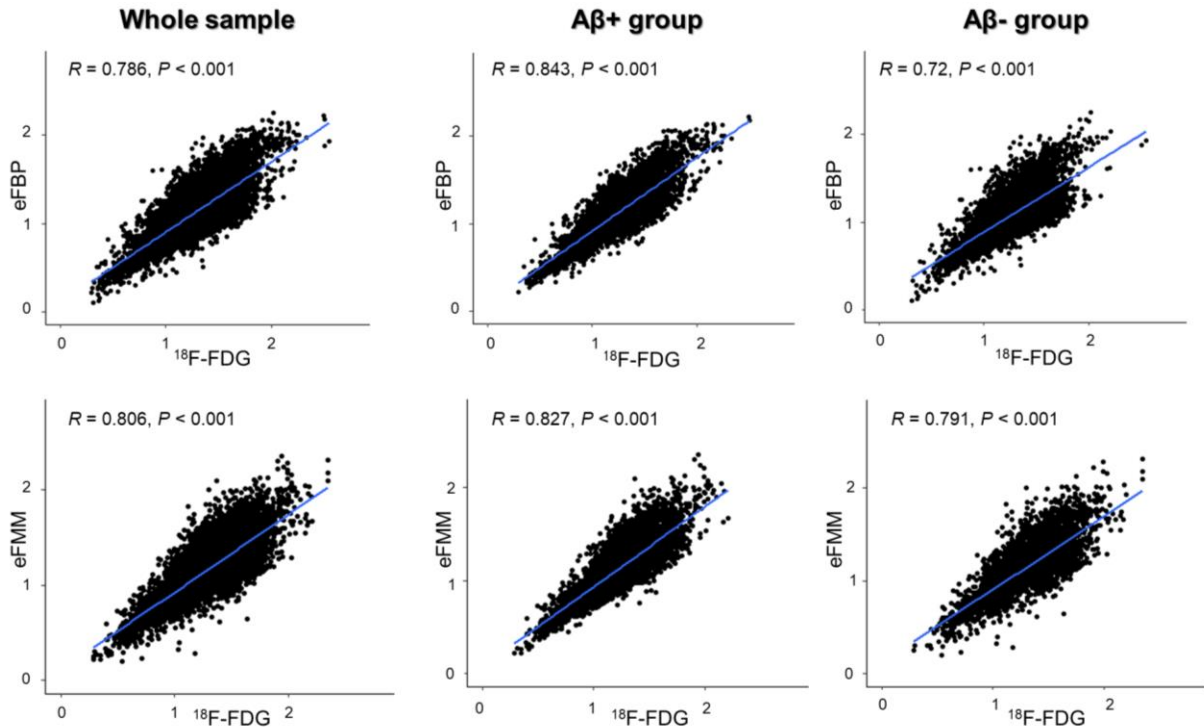


**Figure 1 Correlation between eFBP/eFMM and <sup>18</sup>F-FDG-PET SUVR.** Scatter plots show the association between eFBP/eFMM SUVR (y-axis) in the AAL regions, and their respective FDG SUVR (x-axis). Results are presented for the whole sample (first column) and separately for the subgroups divided according to the amyloid status (second and third columns). Lines resulting from the linear regression are shown in blue. R and *p*-values are given in the upper left corner. Abbreviations: FBP= florbetapir, FMM= flutemetamol, eFBP= early FBP, eFMM= early FMM, Aβ- = amyloid negative, Aβ+ = amyloid positive.

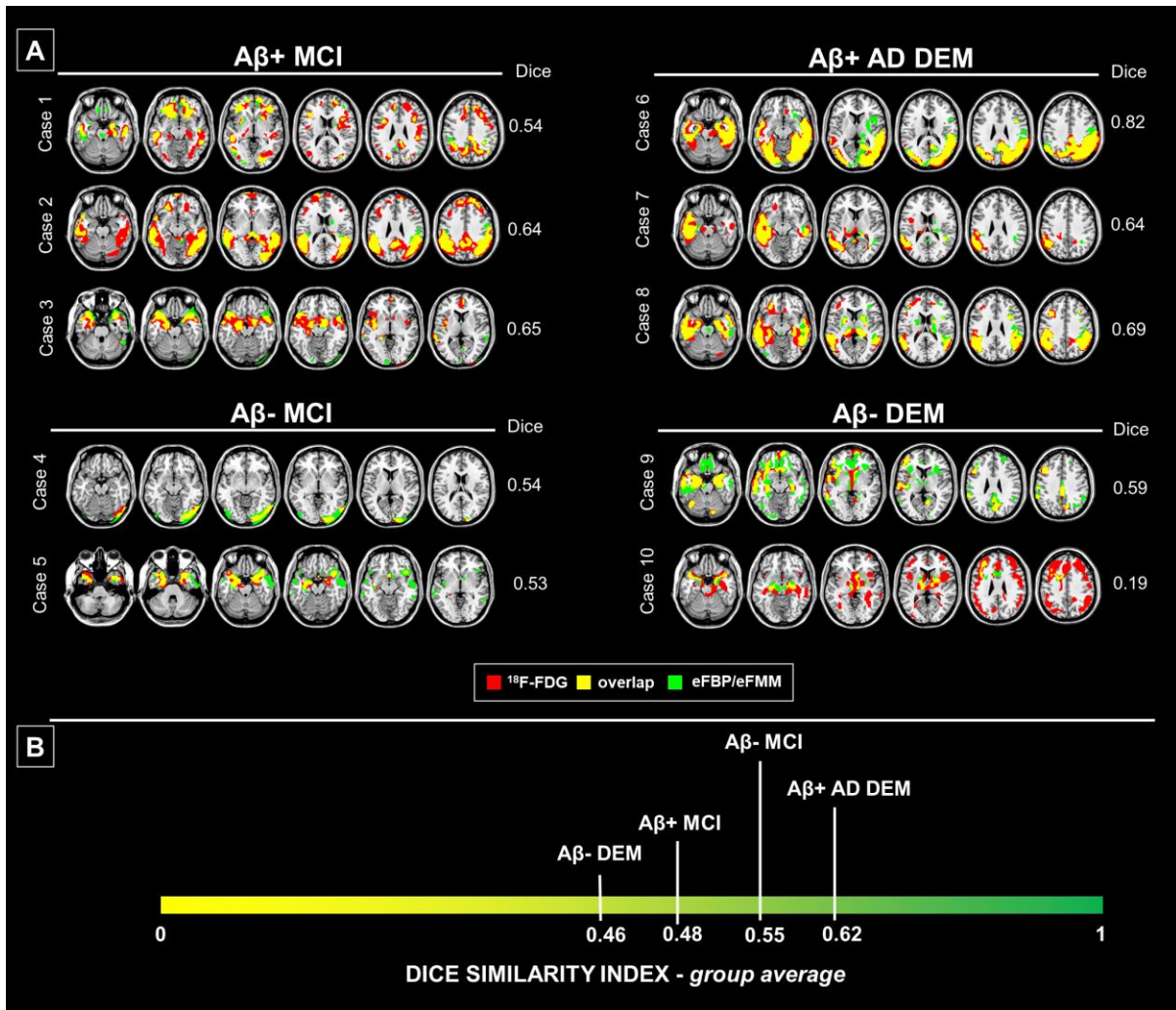


**Figure 2 Hypometabolic and hypoperfusion patterns at the single-subject level.** Panel A shows patterns of  $^{18}\text{F}$ -FDG-PET hypometabolism and eFBP/eFMM hypoperfusion in single individuals. Hypometabolism maps (red), hypoperfusion maps (green), and their overlap (yellow) were over imposed on a standard MNI template. These maps were obtained from the binarization of single-subject  $^{18}\text{F}$ -FDG-PET SPM-t maps and eFBP/eFMM SPM-t maps ( $p < 0.05$  uncorrected,  $k > 100$ ). The Dice similarity index is reported to the right of the brain template of each subject. In panel B, clinical groups are ordered according to the degree of similarity between brain hypometabolism and hypoperfusion, as measured by Dice similarity index average. Lower-to-high (yellow-to-green) values of Dice indicate the increasing degree of overlap. Abbreviations: eFBP= early florbetapir, eFMM= early flutemetamol, A $\beta$ + = amyloid positive, A $\beta$ - = amyloid negative, AD= Alzheimer's disease, MCI= Mild Cognitive Impairment, DEM= dementia.

### A+ N+ AD continuum vs HC

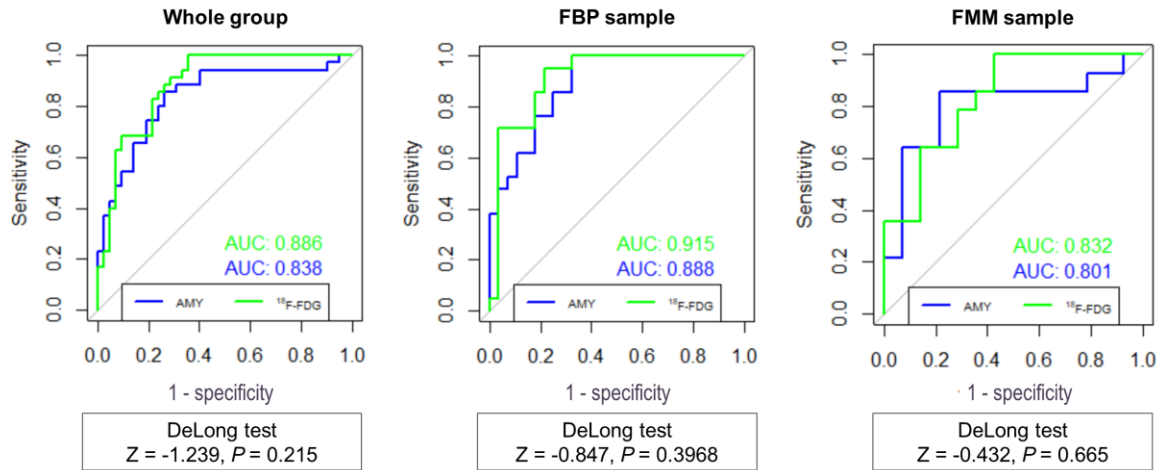


**Figure 3 Discriminative performance of eFBP/eFMM and <sup>18</sup>F-FDG-PET SUVR.** ROC curves show the diagnostic performance of <sup>18</sup>F-FDG-PET and eFBP/eFMM SUVR in composite AD metaROI for distinguishing AD patients from HC. The results are reported for the whole group (first row) and separately for the FBP and FMM samples (second and third rows). AUCs for eFBP/eFMM and <sup>18</sup>F-FDG-PET are shown in blue and green, respectively. Results of the De Long test comparing two AUCs (eFBP/eFMM vs <sup>18</sup>F-FDG-PET) are given in the bottom box. Abbreviations: AUC= area under the curve, FBP= florbetapir, FMM= flutemetamol, AD= Alzheimer’s disease, A+= amyloid positive, N+= neurodegeneration positive, HC= healthy controls.

## Tables

**Table 1** Demographic characteristics of subjects

	<b>Whole sample</b>	<b>FBP group</b>	<b>FMM group</b>	<i>p-value</i>
<b>N</b>	166	94	72	
<b>Age</b> (mean±SD)	73,18±6,35	74,27±5,548	71,76±7,068	<i>p=0,012</i>
<b>gender</b> (F/M)	98/68	58/36	40/32	<i>p=0,425</i>
<b>MMSE</b> (mean±SD)	25,92±4,00	26,12±3,857	25,66±4,202	<i>p=0,471</i>
<b>Aβ status</b> (negative/positive)	70/93	39/52	31/41	<i>p=0,980</i>
<b>Clinical groups (N)</b>				
<b>according to Aβ status</b>				
Aβ+ Alzheimer's Dementia	18	13	5	
Aβ- Dementia	3	2	1	
Aβ+ Mild Cognitive Impairment	52	31	22	
Aβ- Mild Cognitive Impairment	21	9	11	
Aβ+ Cognitively Unimpaired	30	11	19	
Aβ- Cognitively Unimpaired (HC)	42	28	14	

*The p-values reported are resulted from a t-test comparing data from the FBP and FMM subgroups.*

*Abbreviations: FBP= florbetapir, FMM= flutemetamol, N=number, SD= standard deviation, F=females, M=males, MMSE= Mini-Mental State Examination, Aβ- = amyloid negative, Aβ+ = amyloid positive, HC= healthy controls*



**Table 2** The contingency table reporting the frequency of different hypometabolism and hypoperfusion patterns in the whole sample

<b>Hypometabolism patterns classification</b>	<b>Hypoperfusion patterns classification</b>						<b>Total</b>
	<i>AD-like</i>	<i>FTD-like</i>	<i>DLB-like</i>	<i>limbic-like</i>	<i>Unclassified</i>	<i>Normal</i>	
<i>AD-like</i>	30	1	0	4	2	2	39
<i>FTD-like</i>	0	9	0	1	0	0	10
<i>DLB-like</i>	0	0	3	0	0	0	3
<i>limbic-like</i>	0	0	0	14	0	0	14
<i>Unclassified</i>	0	0	0	1	24	1	26
<i>Normal</i>	2	0	0	0	1	29	32
<b>Total</b>	32	11	2	19	28	32	124

*Abbreviations: AD= Alzheimer disease, FTD= frontotemporal disease, DLB= Lewy bodies disease*

**Table 3** The distribution of hypometabolism patterns and their voxel-by-voxel concordance with hypoperfusion maps in clinical groups

FDG pattern classification	<b>Dementia sample (N=21)</b> <i>Aβ (+/-)</i>	Dice average ± SD	% visual match	<b>MCI sample (N=73)</b> <i>Aβ (+/-)</i>	Dice average ± SD	% visual match	<b>CU sample (N=30)</b> <i>Aβ (+/-)</i>	Dice average ± SD	% visual match	<b>Whole sample (N=124)</b> <i>Aβ (+/-)</i>	Dice average ± SD	% visual match
<b>AD-like</b>	10 <i>10/0</i>	0.632 ± 0.159	90%	25 <i>25/0</i>	0.459 ± 0.178	68%	4 <i>4/0</i>	0.611 ± 0.135	100%	39 <i>39/0</i>	0.516 ± 0.185	77%
<b>FTD-like</b>	5 <i>3/2</i>	0.483 ± 0.201	80%	5 <i>3/2</i>	0.531 ± 0.128	100%	0	/	/	10 <i>6/4</i>	0.507 ± 0.161	90%
<b>DLB-like</b>	0	/	/	3 <i>2/1</i>	0.467 ± 0.236	100%	0	/	/	3 <i>2/1</i>	0.467 ± 0.236	100%
<b>limbic-like</b>	0	/	/	13 <i>9/4</i>	0.504 ± 0.078	100%	1 <i>1/0</i>	0.521	100%	14 <i>10/4</i>	0.504 ± 0.075	100%
<b>Unclassified</b>	6 <i>5/1</i>	0.621 ± 0.071	83%	13 <i>8/5</i>	0.498 ± 0.205	100%	7 <i>7/0</i>	0.381 ± 0.293	86%	26 <i>20/6</i>	0.499 ± 0.217	92%
<b>Normal</b>	0	/	/	14 <i>6/8</i>		86% *	18 <i>18/0</i>		94% *	32 <i>24/8</i>		90% *

\* Percentage of patients consistently negative at FDG and early-phase scans is reported

Abbreviations: SD= Standard deviation; MCI= Mild Cognitive Impairment, CU= cognitively unimpaired; AD= Alzheimer disease, FTD= frontotemporal disease, DLB= Lewy bodies disease

## Graphical abstract

### THE COMPARABILITY OF EARLY-PHASE AMYLOID-PET AND FDG-PET IMAGES

AT GROUP LEVEL

AND

SINGLE-SUBJECT LEVEL

